Structural and catalytic effects of surface loop-helix transplantation within haloalkane dehalogenase family

Martin Marek [a,*], Radka Chaloupkova [a], Tatyana Prudnikova [b], Yukari Sato [c], Pavlina Rezacova [d], Yuji Nagata [c], Ivana Kuta Smatanova [b], Jiri Damborsky [a]

[a] Loschmidt Laboratories, Department of Experimental Biology and RECETOX, Faculty of Science, Masaryk University, Kamenice 5, Bld. A13, 625 00 Brno, Czech Republic
[b] Faculty of Science, University of South Bohemia in Ceske Budejovice, Branisovska 1760, 37005 Ceske Budejovice, Czech Republic
[c] Graduate School of Life Sciences, Tohoku University, 2-1-1 Katahira, 980-8577 Sendai, Japan
[d] Institute of Molecular Genetics, Academy of Sciences of the Czech Republic, 142 20 Prague, Czech Republic

ARTICLE INFO

ABSTRACT

Engineering enzyme catalytic properties is important for basic research as well as for biotechnological applications. We have previously shown that the reshaping of enzyme access tunnels via the deletion of a short surface loop element may yield a haloalkane dehalogenase variant with markedly modified substrate specificity and enantioselectivity. Here, we conversely probed the effects of surface loop-helix transplantation from one enzyme to another within the enzyme family of haloalkane dehalogenases. Precisely, we transplanted a nine-residue long extension of L9 loop and α4 helix from DbjA into the corresponding site of DbeA. Biophysical characterization showed that this fragment transplantation did not affect the overall protein fold or oligomeric state, but lowered protein stability (ΔT_m = −5 to 6 °C). Interestingly, the crystal structure of DbeA mutant revealed the unique structural features of enzyme access tunnels, which are known determinants of catalytic properties for this enzyme family. Biochemical data confirmed that insertion increased activity of DbeA with various halogenated substrates and altered its enantioselectivity with several linear β-bromoalkanes. Our findings support a protein engineering strategy employing surface loop-helix transplantation for construction of novel protein catalysts with modified catalytic properties.

1. Introduction

Enzymes catalyse nearly all chemical reactions that occur inside the biological systems [1,2]. As effective biocatalysts, enzymes increase the rates of reactions by lowering their activation energy. A wide range of enzymes are being successfully incorporated into various biomedical, environmental and industrial technologies [3–5]. However, natural enzymes often do not fully meet demands of technological processes, and therefore protein engineering is being applied to improve their catalytic, physico-chemical and thermodynamic properties [6,7]. Enantioselectivity is one of the key parameters for biocatalytic application of enzymes. Enantioselectivity is an ability of a biocatalyst to catalyse chemical reaction, which leads to the formation of one enantiomer of a chiral product [8–10].

Haloalkane dehalogenases (HLDs; EC 3.8.1.5) are microbial α/β-hydrolases that catalyse hydrolytic cleavage of carbon-halogen bond in diverse halogenated aliphatic hydrocarbons via S_N2 reaction. The initial reaction step is followed by the addition of water, releasing a halide ion, a proton, and the corresponding alcohol as the reaction products [11]. Structurally, HLDs are composed of an α/β-hydrolase main domain with a central eight-stranded β-sheet surrounded by six α-helices, and a conformationally malleable helical cap domain [11,12]. The enzyme active site contains five catalytically important amino acid residues, the so-called catalytic pentad. The active site is located in a hydrophobic pocket buried between the main domain and the cap domain. In all HLDs, the active site is connected with the bulk solvent via the main and slot access tunnels, both of them being crucial determinants of catalytic activity, substrate specificity and enantioselectivity [13,14]. The catalytic pentad of HLDs consists of an aspartate nucleophile, a histidine base, a catalytic acid, and two halide-stabilizing residues, mostly tryptophan-tryptophan or tryptophan-asparagine pair [11].

First experiments with HLD enzymes DhlA from *Xanthobacter autotrophicus* and DhaA from *Rhodococcus rhodochrous* NCIMB13064 revealed a moderate enantioselectivity (enantiomeric ratio, *E* value <9) towards haloesters, 1,2-dihaloalkanes and 1,3-dihaloalkanes [15]. A systematic study by Prokop and co-workers showed that haloalkane dehalogenases DhaA, LinB from *Sphingobium japonicum* UT26 and DbjA from *Bradyrhizobium japonicum* USDA110 possess excellent enantioselectivity for α-bromoesters [16]. Moreover, DbjA displayed also high enantioselectivity with two β-bromoalkanes. A sequence comparison suggested that the high enantioselectivity of DbjA arises from a 9-residue EB insertion in L9 loop (Extra region of *B. japonicum*). This insertion connects the α/β-hydrolase core domain with the helical cap domain and is involved in the shaping of both the main and the slot access tunnels [16,17]. Indeed, we have previously demonstrated that the partial deletion (7 amino acids) of EB fragment dramatically changed DbjA enzyme enantioselectivity [16]. Surprisingly, we observed a different impact of the deletion on different substrates: while the enantioselectivity with 2-bromopentane was decreased, the enantioselectivity with methyl-2-bromobutyrate was increased [16]. Crystallographic analysis of the engineered DbjA with deleted EB fragment revealed altered shape and size of the active-site cavity, predominantly due to the modulated conformational behaviour of H139 [16]. The residue H139 is located next to the EB fragment, and in the wild-type DbjA adopts either a flipped-out or a flipped-in conformation. The deletion of EB region constrained H139 in its flipped-in conformation, which caused the dramatic changes in enzyme enantioselectivity [16,18].

In this study, we engineered a haloalkane dehalogenase DbeA from *Bradyrhizobium elkanii* USDA94 [19,20] to further explore structural and catalytic effects of protein surface loop engineering in HLDs. Our previous crystallographic analysis showed that DbeA is a dimeric enzyme with two halide-binding sites present in each protomer, which makes this enzyme unique among all so-far studied HLDs [20]. The DbeA enzyme is closely related to DbjA, but it lacks the 9-residue-long EB insertion in L9 loop and α4 helix [16]. We were therefore interested to see how a transplantation of the DbjA-specific EB fragment into DbeA will affect its catalytic properties.

Here, in order to understand the importance of the extra EB fragment on enzyme functionality, two versions of the fragment equivalent to the extra sequence of DbjA, V_{143}AEEQDHAE and E_{142}-VAEEQDHA, were inserted between D142 and A143 or H141 and D142 of DbeA, respectively, resulting in DbeA-M1 and DbeA-M2 variants. We show that the fragment transplantation did not affect the overall protein fold or the oligomeric state, but it caused a moderate decrease in protein thermal stability. The crystal structure of DbeA-M1 mutant revealed specific structural features of access tunnels, suggesting potential changes in catalytic activity and enantioselectivity. Indeed, our biochemical data show that DbeA-M1 and DbeA-M2 mutants are more active than original wild-type DbeA enzyme but retained its substrate specificity. Moreover, we observed significantly decreased enantioselectivity with 2-bromopentane and increased enantioselectivity with 2-bromohexane. Taken together, our findings support a protein engineering strategy employing surface fragment transplantation to develop new biocatalysts with modified catalytic properties.

2. Results

2.1. Surface fragment engineering does not disrupt the global protein fold

Correct folding of DbeA and DbjA enzyme variants was assessed by measurement of their CD spectra followed by their comparison with the spectra of wild type enzymes. Far-UV CD spectra with typical two negative peaks at 222 and 208 nm of all analysed enzymes indicate their proper folding (Fig. 1), which is a prerequisite for biocatalytic activity. There is an apparent intensity difference between the CD spectra obtained for DbeA and its mutants (DbeA-M1 and DbeA-M2), while the CD spectra of DbjA and its DbjA-M1 mutant are almost identical (Fig. 1A-B). This indicates that the engineered insertions have a slight effect on the specific packing of amino acids forming α-helical structure in DbeA mutants. On the other hand, deletion of seven amino acid residues in DbjA had no effect on its secondary structure (Fig. 1B). The near-UV CD spectra of constructed mutants are identical to those of the corresponding wild-type enzymes, which confirm that the introduced mutations caused no effect on overall protein tertiary structure (Fig. 1C-D). Thermal unfolding experiments were carried out to uncover whether introduced mutations have any effect on protein's thermal stability. Thermal stability was evaluated by determination of melting temperature (T_m). Experimentally determined T_m values showed that all engineered proteins were less thermally stable than their corresponding wild type enzymes (Fig. 1C). The insertion mutations in DbeA decreased thermal stability by 5–6 °C, and the seven-residue deletion in DbjA by 4 °C.

Next, we applied analytical size-exclusion chromatography and native protein electrophoresis to probe whether the insertion/deletion events could affect oligomeric state of generated DbeA and DbjA mutant forms. Wild-type DbeA and DbjA form predominantly dimeric structures [16,20]. We determined molecular weights of DbeA-M1, DbeA-M2, and DbjA-M1 mutants along with wild-type dimeric enzymes DbeA and DbjA, as well as prototype monomeric dehalogenase LinB from *Sphingobium japonicum* UT26. Our results prove that the engineered DbeA and DbjA mutants exist as dimers in solution, analogously to their corresponding wild-type enzymes (Fig. 1D). Taken together, biophysical characterization show that the engineering of surface molecular elements did not affect the overall protein fold or the oligomerization state, but it caused a moderate decrease in thermal stability.

2.2. Crystal structure of DbeA-M1 mutant is intact and correctly folded

Through intensive efforts, we were able to obtain well-diffracting crystals of only DbeA-M1. In this mutant, 9-residue sequence fragment V_{143}AEEQDHAE of DbjA was introduced between the residues D142 and A143 of DbeA (Fig. 2A). The DbeA-M1 crystals diffracted up to 2.2 Å resolution and belonged to monoclinic *C*2 space group with refined unit cell parameters: *a* = 133.75, *b* = 75.13, *c* = 77.60, α = γ = 90.0° and β = 91.9° (Table 1). The structure was solved by molecular replacement, using DbeA wt structure as a search model. The initial model was further refined by several cycles of manual building and automatic refinement. The final model contains one DbeA-M1 dimer (chains A and B with r.m.s.d. on Cα's of 0.3 Å) in the asymmetric unit with 5051 non-hydrogen protein atoms, 415 water molecules, 4 Cl ions and 2 acetate ions originated from crystallization mother liquor. The final model has good deviations from ideal geometry, with R-work and R-free values of 17.49% and 23.54%, respectively (Table 1). The electron density map of DbeA-M1 allowed the positioning of residues 6 to 310 in chain A and residues 5 to 309 in chain B, respectively. Most of the residues could be unambiguously built in density, except for one residue (E145) in chain A and two residues (E145 and E146) in chain B in a disordered L9 loop preceding the α4 helix. Complete crystallographic and refinement statistics are summarized in Table 1.

The structure of DbeA-M1 dimer is very similar to that of wild-type DbeA [20] with r.m.s.d. of 0.65 Å (Fig. 2). The main domain of DbeA-M1 adopts a characteristic α/β-hydrolase fold, with a central twisted 8-stranded β-sheet, where β2 strand is in antiparallel ori-
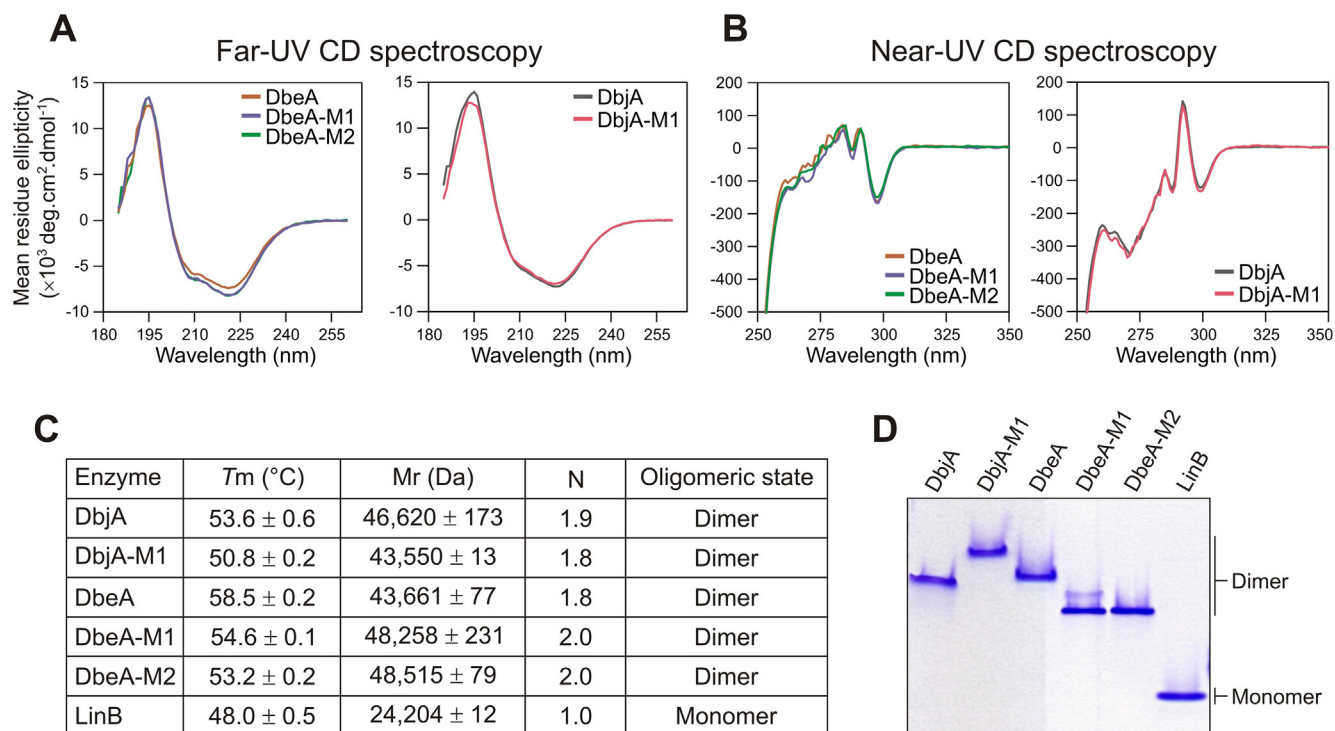
Fig. 1. Biophysical characterization. (A, B) Analysis of correct folding of DbeA, DbeA-M1 and DbeA-M2 (left panels) and DbjA and DbjA-M1 (right panels) by circular dichroism spectroscopy in farUV (A) and near-UV (B) spectral regions. (C) Thermal stabilities and SEC-determined molecular weights of DbeA, DbjA and their mutants (DbeA-M1, DbeA-M2 and DbjA-M1). The thermal stability of enzymes was evaluated by determination of the melting temperature (Tm). Molecular weights (Mr) of DbjA, DbjA-M1, DbeA, DbeA-M1 and DbeA-M2 are approximately two-fold higher (N = ~2) compared to monomeric LinB (N = 1), which demonstrates that these enzymes occur as dimers in the solution. Shown values are means ± standard deviations of three independent measurements. (D) Native polyacrylamide gel electrophoresis of DbjA, DbjA-M1, DbeA, DbeA-M1 and DbeA-M2, and LinB.

entation. The central β-sheet is sandwiched by seven α-helices; namely α1, α10 and α11 helices on one side and α2, α3, α8 and α9 helices on the other side. The α11 helix and β8 strand together form a shallow groove that functions as a major homodimerization interface (Fig. 2C), similar to those previously observed in DbeA and DbjA enzymes [16,20]. The cap domain is composed of five short α-helices (α4, α5́, α5, α6 and α7), which are connected by the surface-exposed loops. The cap domain is inserted between β6 strand and α8 helix and shields the top edge of α/β-hydrolase domain, which contributes to the formation of buried active site. The active site of DbeA-M1 consists of the canonical HLD catalytic pentad: the catalytic base H280, the catalytic nucleophile D103, the catalytic acid E132, and two halide-stabilizing residues N38 and W104 (Fig. 2D). There is an unambiguous density for first chloride anion (Cl1), which is bound in the canonical halide-binding site and it is coordinated by N38 (~3.3 Å), W104 (~3.3 Å), P214 (~3.4 Å) and a water molecule (~3.0 Å). The second chloride anion (Cl2) is located ~10 Å from the Cl1, and it is coordinated by G37 (~3.1 Å), T40 (~3.0 Å), Q102 (~3.2 Å) and Q283 (~3.5 Å) (Fig. 2D). Binding of the second chloride anion (Cl2) to DbeA structure has been shown to have a positive effect on enzyme stability and catalytic activity [20].

2.3. Structural comparisons reveal that DbeA-M1 has unique anatomy of access pathways

The DbjA-specific element V$_{143}$AEEQDHAE, inserted between the residues D142 and A143 of DbeA, triggered an extension of an N-terminal part of the cap domain in DbeA-M1. This region is known to be important for substrate binding and transport of ligands during biocatalysis [16]. The crystal structure of DbeA-M1 mutant reveals that the 9-residue insertion caused the appar-

ent extension of DbeA-M1 α4 helix, which is directly associated with the conformational change of L9 loop connecting β6 strand and α4 helix (Fig. 3A,D). This is the only region where structural changes are observed between the parental DbeA and engineered DbeA-M1 mutant. The structural information is in agreement with the CD analysis, where we also observe that DbeA-M1 and DbeA-M2 mutants have more residues contributing to the α-helical content (Fig. 1).

Interestingly, structural comparison shows that the extended α4 helix in DbeA-M1 is similar, but not identical, to that of DbjA (Fig. 3B,E). The N-terminal part of DbjA α4 helix displays obvious bending leading to distortion of regular α-helical geometry. Strikingly, this is not the case in DbeA-M1 α4 helix, which is straight. As a consequence, the adjacent L9 loop adopts different conformation in DbjA compared to that of DbeA-M1. Moreover, the DbeA-M1 L9 loop is disordered and is not seen entirely in electron density map (Fig. 3 and Fig. S1), which might point towards its higher flexibility, although crystal packing has to be also taken into account. It has been previously reported that side chain of H139 in DbjA L9 loop can adopt either the flipped-in or flipped-out conformation. The structure of DbeA-M1 reveals that H139 in both chain A and B is adopting only the flipped-in conformation, similarly to those observed in DbeA and DbjA-M1 (Fig. 3).

In DbeA-M1, the orientation of E146 in α4 helix is stabilized by a hydrogen bond with H141 (Fig. S2). In addition, H141 is stabilized by a hydrogen bond with Q140, which forms another hydrogen bond with D142. In DbjA, the orientation of E146 is not stabilized by similar hydrogen bonding. Instead, V143 is stabilized by a hydrogen bond formation with T141 (Fig. S2). T141 is further stabilized by E142, which is also interacting with V143 via a hydrogen bonding. In His-DbjA, V143 and Q147, but not E146, are stabilized by hydrogen bond formation with T141. Therefore, we think
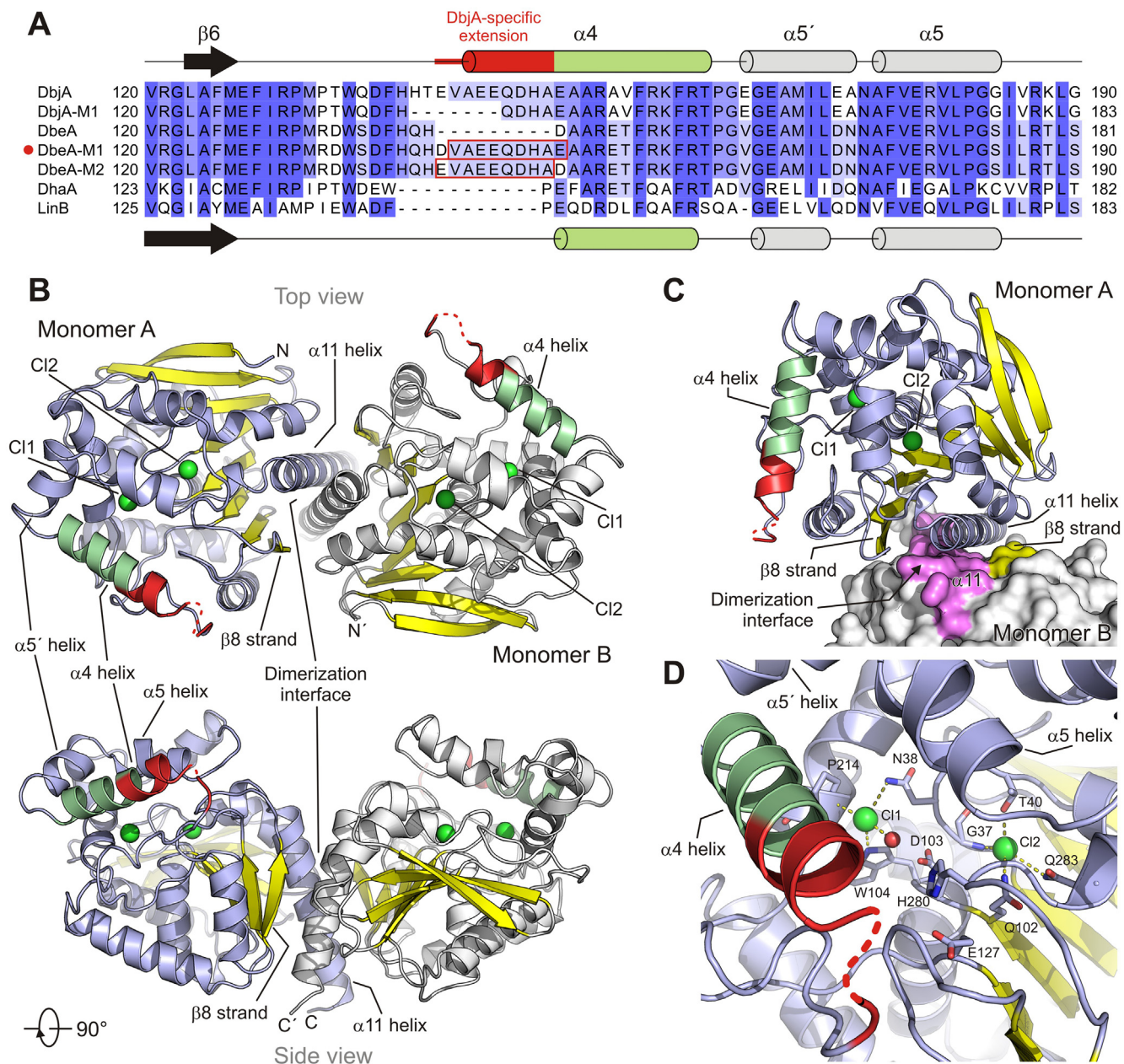
Fig. 2. Structure of DbeA-M1. (A) Partial structure-based sequence alignment of DbjA, DbjA-M1, DbeA, DbeA-M1, DbeA-M2, DhaA and LinB. Sequence identities are shown by levels of blue. Secondary structure elements found in DbjA and LinB are shown above and below the alignment, respectively. Red boxes show the regions that have been transplanted from DbjA to DbeA in the mutational analysis resulting in mutants DbeA-M1 and DbeA-M2. (B) Cartoon representation of overall structure of DbeA-M1 dimer (monomer A in light blue and monomer B in grey colour). The green spheres represent chloride ions (Cl1 and Cl2). The α4 helix is coloured in pale green and the transplanted region from DbjA is coloured in red; for clarity the central β-sheet is coloured in yellow. (C) Zoom in view of the dimerisation interface. The two Dbe-M1 enzyme molecules interact with each other via the shallow groove shaped by α11 helix (violet) and β8 strand (yellow). (D) Close-up view of the enzyme active site. Residues participating in catalysis and chloride binding are shown as sticks. Two chloride ions are shown as green spheres, and a water molecule as red sphere. Yellow dashed lines represent coordinating interactions. (For interpretation of the references to colour in this figure legend, the reader is referred to the web version of this article.)

that the hydrogen bond network involving H141 may be the cause of structural difference in α4 helix between DbeA-M1 and DbjA.

Collectively, our comparative analysis demonstrates that the introduction of DbjA-specific sequence element (V_{143}AEEQDHAE) into DbeA resulted in a new enzyme chimera that displays unique structural features.

2.4. Surface loop-helix engineering resulted in increased activities with halogenated substrates

Enzymatic activities of mutants DbeA-M1, DbeA-M2, DbjA-M1 along with wild-type enzymes DbeA, DbjA, LinB and DhaA, were

measured with a previously established set of representative chlorinated, brominated and iodinated hydrocarbons [21]. Determined specific activities of the enzymes are summarized in Fig. 4 and Table S1. Interestingly, DbjA displayed higher activity than DbeA towards all tested compounds except for 1,3-diiodopropane (54). DbjA was more active than DbjA-M1 except 1,3-diodopropane (54), 1-bromo-2-chloroethane (137) and 1,2-dibromo-3-chloropropane (155). DbeA, DbeA-M1 and DbeA-M2 were under tested conditions inactive with five substrates (Table 2) 1,2-dichloroethane (37), 1,3-dichloropropane (38), 1,2-dichloropropane (67), 1,2,3-trichloropropane (80) and chlorocyclohexane (115). The highest activity of DbeA was observed towards

Table 1
Crystallographic data collection and refinement statistics.

Data collection*	DbeA-M1
Wavelength (Å)	0.918
Space group	C121
Cell dimensions	
a, b, c (Å)	133.75, 75.13, 77.60
α, β, γ (°)	90.00, 91.90, 90.00
Resolution (Å)	19.60–2.20 (2.27–2.20)
Total reflections	145,196 (22,532)
Unique reflections	38,810 (6037)
Rmerge	13.8 (51.5)
I/σI	11.76 (3.35)
Completeness (%)	98.6 (96.4)
Multiplicity	3.74 (3.73)
CC(1/2)	86.3 (62.8)
Wilson B-factor	32.3
Refinement	
Resolution (Å)	19.60–2.20 (2.27–2.20)
No. reflections	36,818 (2264)
Rwork/Rfree	17.49/23.54
Number of atoms	
Protein	4629
Ligand	8
Water	415
B-factors	
Protein	31.68
Ion Cl1	21.85
Ion Cl2	27.42
R.m.s deviations	
Bond lengths (Å)	0.0188
Bond angles (°)	1.8784
Ramachandran favoured (%)	96.2 (581/604)
Ramachandran allowed (%)	100 (604/604)
Ramachandran outliers (%)	0 (604/604)
PDB ID code	6XY9

*Values in parentheses are for the highest-resolution shell.

1,3-diiodopropane (54), whereas the highest activity of DbeA-M1 (Fig. 4C) was observed towards 1-bromobutane (18), 1-bromohexane (20) and 1,3-dibromopropane (48). Activity of DbeA-M1 was slightly higher than activity of DbeA-M2, but overall activities of both enzymes are very similar (Fig. 4B). Both DbeA insertion mutants (DbeA-M1 and DbeA-M2) had higher activity towards 1-bromobutane (18), 1-bromohexane (20) and 1,3-diiodopropane (54) than DbjA (Fig. 4E).

The enzymes DbjA and LinB exhibited higher activity than other enzymes (Fig. 5A-B), according to first PCA analysis with raw data. The PCA carried out with absolute values of activities was in the direction of the first component generally influenced by the magnitude of activity of individual enzymes with analysed substrates. The deletion of 7-residue-long element in DbjA had a significant effect on the activity of DbjA-M1, which decreased significantly in comparison with wild-type DbjA [16]. In contrast, the insertion of 9-residue-long element into DbeA-M1 and DbeA-M2 increased activities with all substrates (Fig. 5A) with the exception for 1,3-diiodopropane (54).

The PCA analysis (Fig. 5C-D) with standardized data enabled the comparison of the enzyme activity profiles. The first component separated HLDs according to their preference to halogenated compounds. Mostly chlorinated substrates substituted at vicinal positions were located on the left side of the component 1 (Fig. 5D). These substrates were generally better converted by LinB, DhaA, DbjA and DbjA-M1. Brominated and iodinated compounds substituted on terminal positions were better converted by DbeA and its loop mutants DbeA-M1 and DbeA-M2. Chlorinated compounds are generally worse substrates for DbeA and its mutants. Several chlorinated substrates were not converted by these enzymes at all. The deletion of 7 residues in DbjA had a significant effect on the substrate specificity of DbjA-M1, which significantly changed

due to the loss of activity with 1,2-dichloroethane (37), 2-iodobutane (64), 1,2-dichloropropane (67), 1,2,3-trichloropropane (80) and due to the acquisition of new activity towards 1,2-dibromo-3-chloropropane (155). DbeA-M1 and DbeA-M2 showed no obvious changes in substrate specificities under used experimental conditions (Fig. 5C).

2.5. Surface loop-helix engineering resulted in modified enantioselectivity with β-substituted bromoalkanes

HLDs show high enantioselective conversion of brominated hydrocarbons into chiral alcohols [16]. Therefore, the influence of the surface loop engineering on enantioselectivity was studied. Kinetic resolutions of a series of racemic substrates catalysed by several HLDs are summarized in Table 2 and Table S2. No significant differences were observed in enantioselectivity of DbjA, DbjA-M1, DbeA, DbeA-M1 and DbeA-M2 with β-substituted halogenated esters except for methyl 2-bromobutyrate (373). DbeA, DbeA-M1 and DbeA-M2 showed reduced enantioselectivity with 2-bromopentane (63) and improved enantioselectivity with 2-bromohexane (178). All enzymes were distributed similarly in the direction of the first component, which was influenced by all analysed substrates (Fig. 5E-F). Distribution along the second component was mainly influenced by the enantioselectivity with substrates 2-bromopentane (63) and 2-bromohexane (178). The deletion of 7-residues-long fragment in DbjA had effect on the enantioselectivity of DbjA-M1 with 2-bromopentane. E-value decreased from 145 for DbjA to 58 for DbjA-M1 with 2-bromopentane. The insertion of 9-residues-long fragment into DbeA significantly decreased enantioselectivity of DbeA-M1 and DbeA-M2 with 2-bromopentane (63), whereas only moderately increased enantioselectivity of DbeA-M1 and DbeA-M2 with 2-bromohexane (178), Table 2.

3. Discussion

We have previously demonstrated that engineering of protein surface loops and access tunnels can significantly modulate enantioselectivity of the haloalkane dehalogenase DbjA [16,18]. This effect was achieved by the deletion of the so-called EB fragment, which is 9-residue-long insertion located in the L9 loop and the α4 helix (Fig. 3B). Our structure–function analysis revealed that the molecular mechanism underlying the changed enantioselectivity of DbjA deletion mutant was connected to reshaped main access tunnel that favoured catalytic conversions of α-bromoester and β-bromoalkane enantiomers [16]. Specifically, the constrained flipped-in conformation of H139, lining the enzyme main access tunnel (Fig. 3F), has been shown to be critical for the observed shift in enzyme enantioselectivity towards β-bromoalkanes [16].

In this study, we transplanted the DbjA-specific EB fragment into a closely related DbeA dehalogenase (Fig. 2A). The purpose of this engineering step was to probe the molecular basis of enzyme-substrate recognition that contributes to enzyme enantioselectivity. Biophysical characterization of the constructed DbeA mutants (DbeA-M1 and Dbe-M2) indicated that the transplantation of EB fragment did not affect the overall protein fold or the oligomeric state, but caused a moderate decrease in thermal stability. The crystal structure of DbeA-M1 mutant showed that the inserted element (V_{143}AEEQDHAE) extended the α4 helix on its amino-terminal end in a similar manner as is observed in DbjA, although with clear differences. While the end of α4 helix in DbjA is distorted towards the α/β-hydrolase core, the corresponding α4 helix in DbeA-M1 is straight (Fig. 3B, E). As a consequence, the adjacent L9 loop is adopting slightly different conformations in DbeA-M1
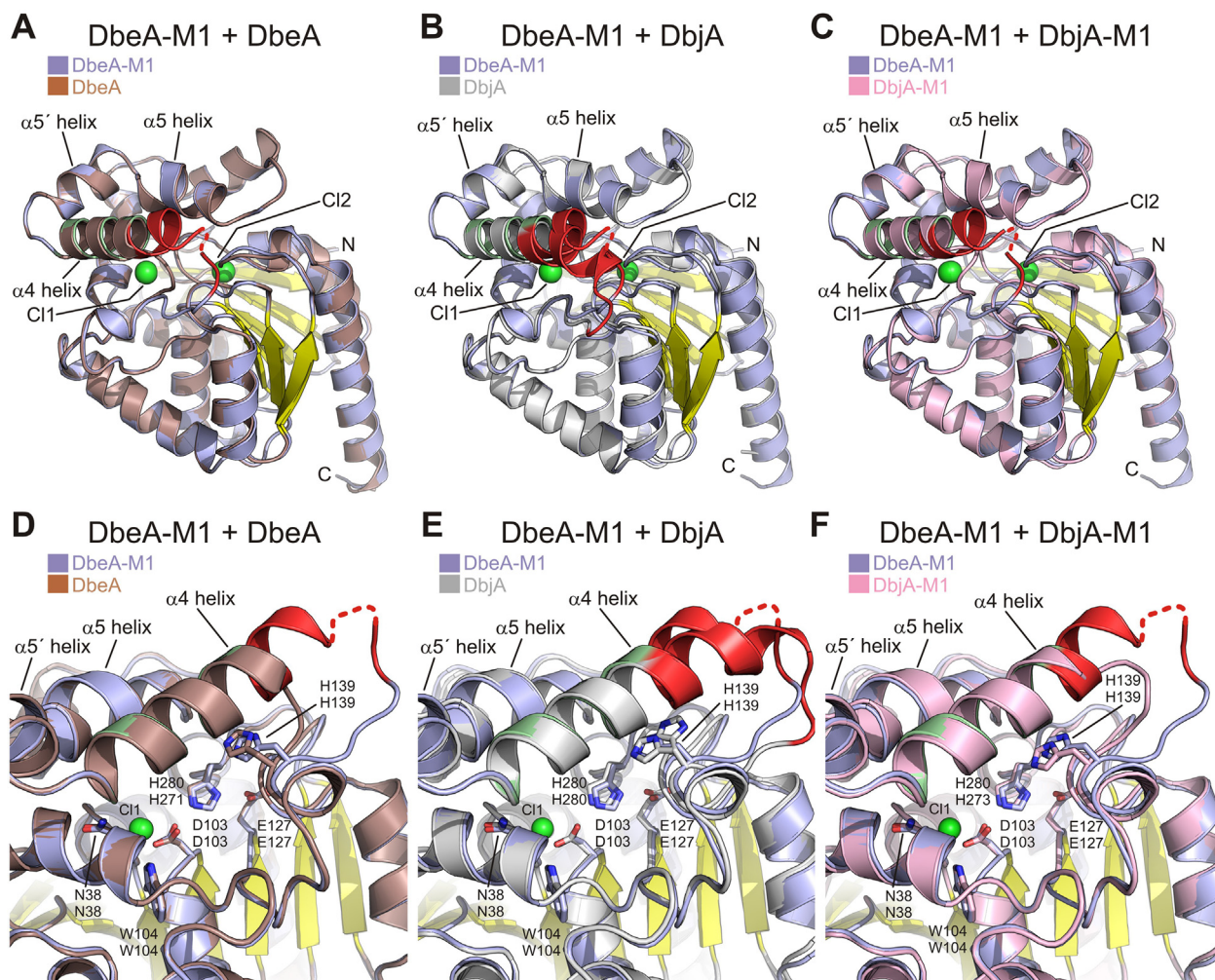
Fig. 3. Structural comparisons of DbeA-M1, DbeA, DbjA and DbjA-M1. Superposition of DbeA-M1 with DbeA (A, D), DbeA-M1 with DbjA (B, E), and DbeA-M1 with DbjA-M1 (C, F). The transplanted region encompassing α4 helix and adjacent L9 loop are coloured in red; the chloride anions (Cl1 and Cl2) bound to enzymes are shown as green spheres. DbeA-M1 H139 adopts a single flipped-in conformation (D), while the corresponding DbjA H139 adopts the both flipped-in and flipped-out conformations (E). (For interpretation of the references to colour in this figure legend, the reader is referred to the web version of this article.)

and DbjA, which might reflect their different catalytic performance and enantioselectivity. Specifically, two amino acid residues (E145 and E146) in the Dbe-M1 L9 loop are not seen in electron density, which suggests that this region is rather conformationally flexible. In addition, our crystallographic analysis showed that the insertion of 9-residue-long EB fragment into DbeA did not affect conformational behaviour of H139, which is entirely present in its flipped-in conformation, similarly to that observed in wild-type DbeA (Fig. 3D). In other words, it means that we were not able to restore conformational freedom of H139 in DbeA through the transplantation of DbjA-specific EB fragment. This finding suggests that there has to be some additional molecular determinant influencing conformational behaviour of H139, besides the DbjA-specific EB fragment. Based on our structural dissection, we think that the hydrogen bond network involving H141 may be the cause of structural difference in α4 helix between DbeA-M1 and DbjA.

The previous study with the DbjA enzyme demonstrated that the removal of its specific EB fragment had a dramatic effect on its catalytic activity, substrate specificity and enantioselectivity [16]. We hypothesised that the transplantation of DbjA-specific EB element into the closely related dimeric DbeA enzyme may result in an enzyme with DbjA-like catalytic properties. In general, the transplantation of the DbjA-specific EB element into DbeA did not cause such dramatic changes in the catalytic activity, speci-

ficity and enantioselectivity, like those observed with deletion mutant of DbjA (Figs. 4 and 5). Yet, we observed that the DbeA-M1 and DbeA-M2 mutants were more active than original wild-type for most of the substrates (Fig. 5). However, both engineered enzymes showed increased enantioselectivity with 2-bromohexane (178) and decreased enantioselectivity with 2-bromopentane (63). These results are in an agreement with study of Sykora and co-workers, who demonstrated that dynamics and hydration of access tunnels profoundly affected the enantioselectivity of haloalkane dehalogenases [22].

In conclusion, we have successfully transplanted the DbjA-specific EB fragment (V$_{143}$AEEQDHAE) into DbeA structure, resulting in engineered enzymes with unique structural and catalytic features. Our findings support a protein engineering strategy employing surface fragment transplantation to create new biocatalysts with unique catalytic properties.

4. Experimental procedures

4.1. Cloning of DbeA mutants

The mutants were generated using standard PCR-based nested protocols and inserted into the pET21b expression vector. The
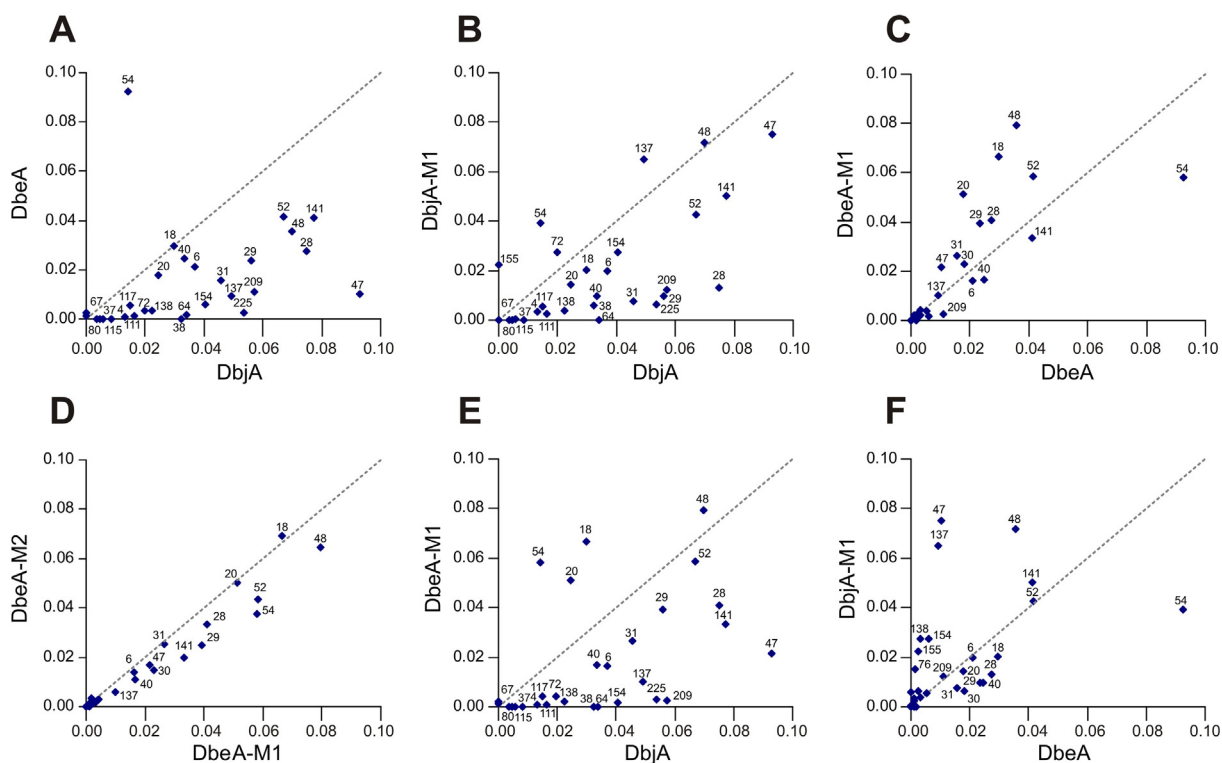
Fig. 4. Comparative plots of enzyme specific activities [$\mu mol.s^{-1}.mg^{-1}$] towards a set of halogenated compounds. (A) DbjA versus DbeA, (B) DbjA versus DbjA-M1, (C) DbeA versus DbeA-M1, (D) DbeAM1 versus DbeA-M2, (E) DbjA versus DbeA-M1, (F) DbeA versus DbjA-M1. The numbering of halogenated compounds is provided in Supplementary Table S1. The greater the similarity between the activities of the two enzymes, the more activity values lie on the line. DbjA is generally more active than DbeA (A), DbjA-M1 (B), and DbeA-M1 (E). DbeA-M1 and DbeA-M2 have very similar activities (D), and they both are interestingly more active towards brominated substrates than DbeA (C) and DbjA (E). DbeA exhibits the highest activity towards 1,3-diiodopropane (no 54) (A, C, F).

Table 2
Kinetic resolution of a series of racemic substrates catalysed by haloalkane dehalogenases DbjA, DbjA-M1, DbeA, DbeA-M1, Dbe-M2, DhaA and LinB. Summary of E-values. The arrows indicate the largest changes in analysed properties.

No.	Compound	DbjA	DbjA-M1	DbeA	DbeA-M1	DbeA-M2	DhaA	LinB
62	2-bromobutane	1	1	1	2	2	2	2
63	**2-bromopentane**	**145**	**58↓**	**91**	**24↓**	**13↓**	**7**	**16**
178	**2-bromohexane**	**68**	**76↑**	**113**	**140↑**	**141↑**	**4**	**12**
179	2-bromoheptane	28	2	2	2	3	3	3
375	methyl 2-bromopropionate	>200	>200	>200	>200	>200	>200	52
373	methyl 2-bromobutyrate	>200	70	0	0	0	0	28
356	ethyl 2-bromopropionate	>200	>200	>200	>200	>200	85	97
348	ethyl 2-bromobutyrate	>200	>200	>200	>200	>200	>200	>200
408	ethyl 2-bromoisovalerate	0	0	0	0	0	0	>200
357	ethyl 2-bromovalerate	0	0	0	0	0	0	46
351	ethyl 2-bromohexanoate	0	0	0	0	0	0	10
159	methyl 3-bromo-2-methylpropionate	20	ND[a]	15	10	9	5	3
410	3-bromo-2-butanone	>200	>200	ND[a]	ND[a]	ND[a]	>200	3
268	2-bromopropiophenone	>200	>200	>200	>200	>200	>200	13
259	2-(bromomethyl)tetrahydro-2H-pyran	12	10	15	0	0	1	3

ND: not determined ; [a] active, but not measured, high amount of enzyme required.
The enantiomeric ratio (E-value) is a quantitative measure of enzyme stereospecificity and is defined as the ratio of the specificity constants (k_{cat}/K_m) towards the (R-) and (S-) enantiomers; $E\text{-}value = (k_{cat}^R/K_m^R)/(k_{cat}^S/K_m^S)$ [22].
The E-values of DbeA, DbeA-M1, DbeA-M2 and DbjA-M1 (except E-values for 2-bromopentane and methyl 2-bromobutyrate) presented in Table 2 were uniquely measured for this study, whereas E-values of DbjA, LinB and DhaA were previously reported by Prokop et al. 2010 [16].

L9-α4 element exchange mutants were designed based on structural comparison. Briefly, for the DbeA-M1 mutant, the DbjA-specific elements encompassing L9 and α4 sequence (V143-AEEQDHAE) was introduced between the residues D142 and A143 of DbeA. For the DbeA-M2 mutant, the DbjA-specific elements encompassing L9 and α4 sequence (E142VAEEQDHA) was introduced between the residues H141 and D142 of DbeA. Briefly, The *dbeA* gene (Genbank accession No. AB478942) was PCR-amplified using primers DbeA-F and DbeA-R and cloned between

HindIII and BamHI restriction sites in pUC19 vector. The resulting plasmid was named pYDE2a. Insertion variants of *dbeA* (*dbeA-M1, dbeA-M2*) was constructed by PCR-amplification of the entire pYDE2a with primer sets DbeA-M1-F and DbeA-M1-R or DbeA-M2-F and DbeA-M2-R (Table S3) and the following phosphorylation and ligation of the PCR products. Nucleotide sequences of dbeA-M1 and dbeA-M2 in pUC19 were confirmed by DNA sequencing. Each gene was then re-cloned between NdeI and XhoI sites of pET21b. DbeA-M1 and DbeA-M2 both contain eight addi-
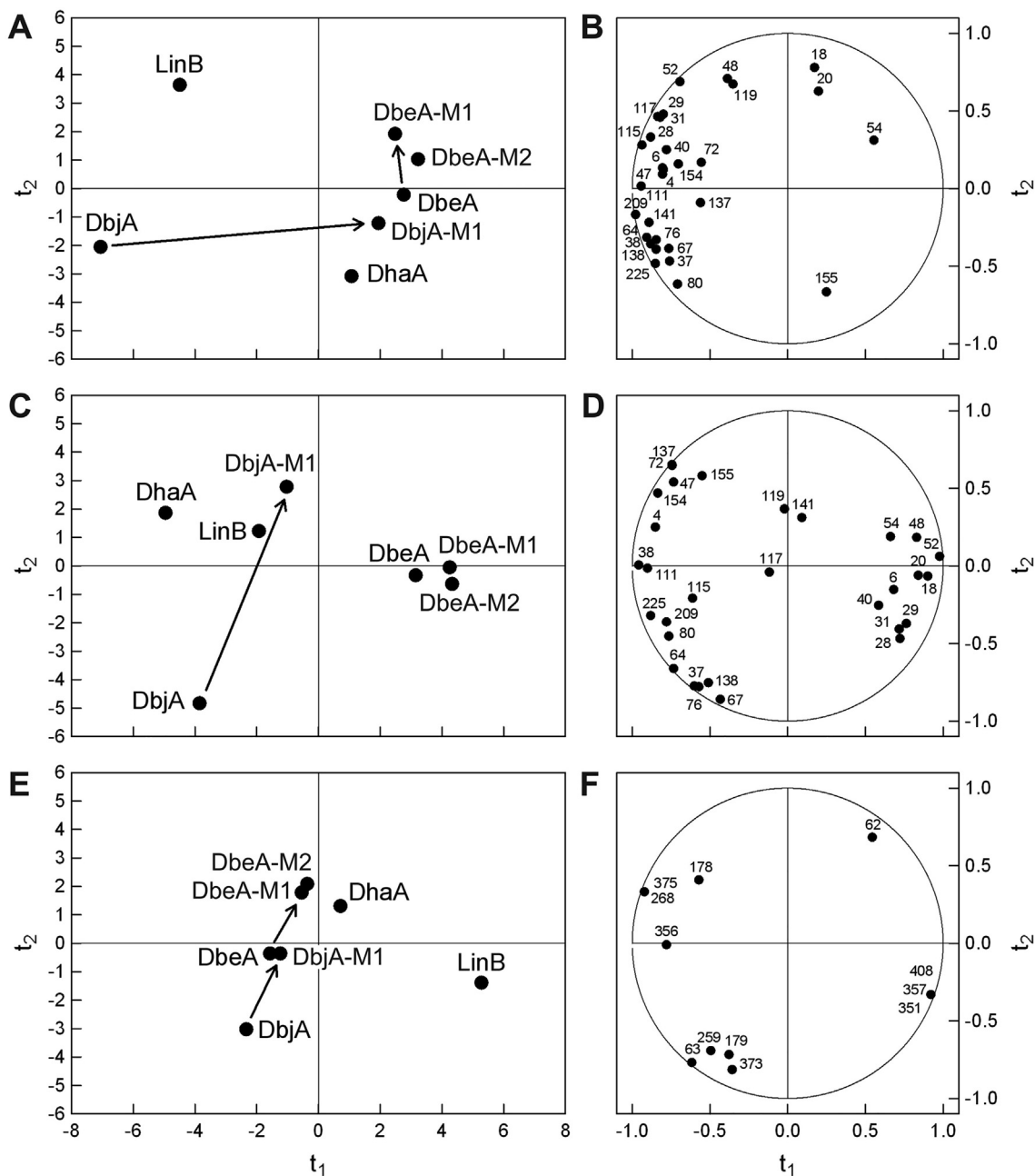
Fig. 5. Statistical analyses of the activity, substrate-specificity and enantioselectivity data. (A) The score plot t_1/t_2 from principal component analysis (PCA) with the untransformed activity data set. The score plot is a two-dimensional window into multidimensional space, where the objects (enzymes) with similar properties (here activities) are collocated. The plot shows differences in the overall activities of individual HLDs towards individual substrates. The overall activity of DbjA-M1 is significantly lower than the activity of the most active HLD-II enzyme DbjA. On the other hand, the overall activity of DbeA-M1 and DbeA-M2 is only slightly modified when compared with DbeA, since both variants exhibited improved activity predominantly towards brominated and iodinated substrates but not towards chlorinated ones. (B) The corresponding loading plot p_1/p_2 from PCA with the untransformed activity data set showing the main substrates for each enzyme. (C) The score plot t_1/t_2 from PCA with the transformed activity data set. The plot shows differences in substrate specificity of individual enzymes, where the enzymes with similar substrate preferences are collocated. While the substrate specificity of both DbeA-M1 and DbeA-M2 is almost identical to that of DbeA, the substrate specificity od DbjA-M1 is significantly modified when compared with its DbjA counterpart due to the variant decreased preference towards disubstituted ethanes and propanes (substrates no 37, 67, 76), β-substituted (substrate no 64) and chlorinated compounds (such as substrates no 4, 38, 80, 115, 209, 225). (D) The corresponding loading plot p_1/p_2 from PCA with the transformed activity data set showing the substrates that govern enzyme clustering. (E) The score plot t_1/t_2 from PCA with the untransformed enantioselectivity data. The plot shows differences in the overall enantioselectivity of the tested enzymes. Overall enantioselectivity of DbjA-M1 is lower than that of DbjA due to the variant decreased enantioselectivity towards 2-bromopentane (no 63), 2-bromoheptane (no 179) and methyl 2-bromobutyrate (no 373). The overall enantioselectivities of DbeA-M1 and DbeA-M2 are lower than that of DbeA since both variants exhibited significantly lower enantioselectivity towards 2bromopentane (no 63). (F) The corresponding loading plot p_1/p_2 from PCA with the untransformed enantioselectivity data showing the tested substrates. The numbering of halogenated compounds used for activity testing is provided in Table S2, the numbering of halogenated compounds used for enantioselectivity testing is provided in Table 2.

tional amino acid residues derived from pET21b sequence (Leu-Glu-His-His-His-His-His-His) at the C-terminus. The DbjA-M1 mutant has been reported previously by Prokop and co-workers

[16]. The sequence comparisons and detailed description of all mutants used in this study are shown in Figs. S3 and S4 and Table S4.

4.2. Protein expression and purification

Recombinant overproduction of HLD enzymes was done as reported previously [16,19,20]. Briefly, all genes coding for corresponding wild-type or enzyme variants were cloned between NdeI and BamHI sites in expression vector pET21b with a hexahistidine affinity tag on carboxy-terminal end. Transformed *Escherichia coli* BL21(DE3) cells were cultured in LB medium at 37 °C until OD_{600} of ~0.6. Protein expression was then induced by addition of isopropyl-β-D-thiogalactopyranoside (IPTG) to a final concentration of 0.2 mM. After induction, the cell culture was incubated at 18 °C for 12 h and then harvested by centrifugation. The cell pellets were re-suspended in a purification buffer (50 mM potassium phosphate buffer supplemented with 500 mM NaCl and 10 mM imidazole, pH 7.5), and cells were disrupted by sonication using the Ultrasonic Processor UP200S (Hielscher, Germany). The lysates were clarified by high-speed centrifugation (100,000 g, 1 h) and supernatants were applied on a Ni-NTA Sepharose column HR 16/10 (Qiagen, Germany). Unbound and weakly bound proteins were washed out by the purification buffer with 37.5 mM imidazole. The His-tagged enzymes were then eluted by a linear gradient of imidazole (37.5–500 mM). The active fractions were pooled and dialysed overnight against 50 mM potassium phosphate buffer, pH 7.5. The enzymes were stored at 4 °C in 50 mM potassium phosphate buffer (pH 7.5) supplemented with 1 mM β-mercaptoethanol and 10% glycerol. Purity of enzymes was analysed by SDS-PAGE (Fig. S5) and protein concentrations were measured by the Bradford protein assay.

4.3. Circular dichroism and thermal denaturation measurements

Circular dichroism (CD) spectra were recorded at room temperature (20 °C) using a Jasco J-810 spectropolarimeter (Jasco, Japan). All of the spectra were obtained at an interval of 0.1 nm with a scanning speed 100 nm/min, 1 s response time and 2 nm bandwidth. Cuvettes of 0.1- and 1-cm path length were used in the far- and near-UV regions, respectively. The protein concentration in potassium phosphate buffer for the far-UV and the near-UV spectra acquisition were 0.2 mg/ml and 4.5 mg/ml, respectively. Each spectrum shown is the average of ten individual scans and is corrected for absorbance caused by the buffer. CD spectra were expressed in terms of the mean residue ellipticity. Thermal unfolding of prepared enzymes was followed by monitoring the ellipticity at 222 nm over the temperature range from 20 to 80 °C, with a resolution 0.2 °C, at a heating rate 1 °C/min. Recorded thermal denaturation curves were roughly normalized to represent signal changes between approximately 1 and 0 and fitted to sigmoidal curves using software Origin 6.1 (OriginLab, Massachusetts, USA). The melting temperatures (T_m) were evaluated as a midpoint of the normalized thermal transition.

4.4. Size-exclusion chromatography

Calibration kit of protein samples LMW and HMW Gel Filtration Kit (GE Healthcare, Sweden) were diluted in 50 mM phosphate buffer (pH 7.5). Haloalkane dehalogenases DbjA, DbjA-M1, DbeA, DbeA-M1, DbeA-M2, LinB and proteins from calibration kit - albumin (Mw = 67,000), chymotrypsinogen A (Mw = 25,000), ribonuclease A (Mw = 13,700) and ovalbumin (Mw = 4300) were analysed using FPLC system equipped with UV_{280} detection (GE Healtcare, Sweden) and Superdex 200 10/300 GL column (GE Healtcare, Sweden). Total volume of 100 µl of each protein sample was applied on the column and separated under constant flow 0.5 ml/min.

4.5. Native polyacrylamide gel electrophoresis

Enzymes DbjA, DbjA-M1, DbeA, DbeA-M1, DbeA-M2, LinB, ovalbumin, albumin and chymotrypsinogen A were diluted to the concentration of 0.5 mg/ml. Protein samples (30 µl) were mixed with 10 µl of Bromophenol blue and 10 µl of mix solution was loaded into wells. Electrophoresis was run under constant current (120 V) for 2 h in cold room (4 °C).

4.6. Enzyme activity assays

Dehalogenating activity of haloalkane dehalogenases DbjA, DbeA, DbeA-M1, DbeA-M2 towards a set of 31 substrates previously assembled by Koudelakova and co-workers [23]. Activities were measured by spectrophotometric assay at 460 nm using the Iwasaki method [24]. Dehalogenation reactions were performed at 37 °C in 25-ml Reacti-Flasks closed by Mininert Valves containing 10 ml of 100 mM glycine buffer (pH 8.6) and 10 µl of halogenated compound. The reaction mixture contained 10 ml glycine buffer (100 mM, pH 8.6) and 10 µl of an appropriate halogenated substrate at a final concentration of 0.1–10 mM depending on the substrate solubility. Enzymatic reaction was initiated after 30 min incubation at 37 °C by addition of 0.08 mg of enzyme. The reaction was monitored by withdrawing 0.5 ml of reaction mixture at 0, 5, 10, 20, and 40 min using a syringe needle to reduce evaporation of the substrate. The samples were immediately mixed with 0.1 ml of 35% nitric acid to stop the reaction. The Iwasakís reagent I (0.1 ml) and II (0.2 ml) were then added to the mixture. These solutions enable quantification of the concentration of halides that are released during the enzymatic reaction. Absorbance was measured by microplate reader (SUNRISE, Japan). Dehalogenation activity of tested enzymes was expressed in the terms of specific activity which is defined as moles of substrate converted per unit time (in our case per second) under given reaction conditions (37 °C, pH 8.6) per milligram of total enzyme present (μmol s^{-1} mg^{-1}).

4.7. Enantioselectivity assays

The enzymatic conversions were performed at room temperature (24 °C) in screw-capped reaction vessels containing 20 ml of 50 mM Tris-sulphate buffer (pH 8.2). The substrates were added to a final concentration of 0.1 to 2.5 mM, depending on the apparent enzyme affinity. Enzymatic reactions were initiated by addition of an appropriate amount of purified haloalkane dehalogenase depending on the specific activity (usually 0.5 to 10 mg of enzyme was added for complete conversion of one enantiomer over a period of 10 to 15 min). The reaction progress was monitored by periodically withdrawing aliquots from the reaction mixture. The samples were extracted with diethyl ether containing 1,2-dichloroethane as an internal standard, dried on a short column containing anhydrous Na_2SO_4 and analysed on a Hewlett-Packard 6890 gas chromatograph (Agilent Technologies, USA) equipped with a flame ionisation detector and chiral capillary columns Chiraldex B-TA and Chiraldex G-TA (Alltech, USA). The enantioselectivity was calculated using the enantiomeric ratio, according to the equation $E = (k_{cat,R}/K_{m,S})/(k_{cat,S}/K_{m,S})$, where k_{cat} and K_m represent the respective Michaelis-Menten parameters of the enantiomers. The enantiomeric ratio (E-value) is a quantitative measure of enzyme stereospecificity and is defined as the ration of the specificity constants (k_{cat}/K_m) towards the (R-) and (S-) enantiomers [25]. To estimate these kinetic parameters, the equations that describe competitive Michaelis-Menten kinetics were fitted by numerical integration to progress curves of substrate concentrations in time obtained from the kinetic resolution experiments by using MicroMath Scientist 2.0 (ChemSW, USA). Kinetic

resolution of 2-bromohexane by haloalkane dehalogenase DbeA and its two variants DbeA-M1 and DbeA-M2 is shown in Fig. S6.

4.8. Principal component analysis (PCA)

The activity data measured with seven HLDs (LinB, DhaA, DbjA, DbjA-M1, DbeA, DbeA-M1 and DbeA-M2) and the set of substrates were adapted for the multivariate analysis. Raw enantioselectivity data without any modification in the scale from 0 to 200 were used for PCA analysis. If no enantioselectivity was determined due to very low enzymatic activity, the E-value was considered to be 0. The highest E-value used in analysis was 200 even if the enantioselectivity was marked as higher than 200. The enantiomeric ratio (E-value) is defined as the ratio of the specificity constants (k_{cat}/K_m) towards the (R-) and (S-) enantiomers [25]. The PCA based on correlations was applied as an investigative tool for the revelation of relationships among HLDs. HLDs were taken into analysis as cases, whereas substrates as variables. PCA was performed with differently treated activity data: (i) with the absolute data and (ii) with the data transformed by decimal logarithm and standardized by dividing by the sum of all activity data for the individual enzymes. The first approach compared HLDs based on magnitudes of activity towards individual substrates, whereas the second method compared HLDs according to their specificities. Statistical analysis was performed using Statistica 8.0 (StatSoft, USA).

4.9. Temperature and pH optimum

Dehalogenation reactions for temperature optimum were performed at 20–60 °C, for pH optimum at 37 °C in 25-ml Reacti-Flasks closed by Mininert Valves. The reaction mixtures for temperature optimum contained 15 ml of 100 mM glycine buffer (pH 8.2), for pH optimum contained 15 ml of Briton-Robinson buffer covering the pH range 5.0–10.3 and 2 μl of substrate 1-iodohexane. The reaction mixtures for temperature optimum contained 15 ml of 100 mM glycine buffer (pH 8.2), for pH optimum contained 15 ml of Briton-Robinson buffer covering the pH range 5.0–10.3 and 2 μl of substrate 1-iodohexane at a concentration 0.3 mM. The reactions were initiated by addition of 132 μg of DbeA enzyme. The reactions were vigorously stirred (150 rpm) and monitored by withdrawing of 1 ml sample at 6, 12, 20, 30 and 60 min from the reaction mixtures. The samples were immediately mixed with 0.1 ml of 35% nitric acid to stop the enzymatic reaction. DbeA activity was assayed by the Iwasaki method [24]. The halide released was measured spectrophotometrically at 460 nm with mercuric thiocyanate and ferric ammonium sulphate using microplate reader (SUNRISE, Japan). Dehalogenating activities were quantified by a slope of the relationship between the product concentration and the time. Data points were measured in 4–6 independent replicates and represented as mean values with plotted standard errors.

4.10. Crystallization and diffraction data collection

The DbeA-M1 enzyme was crystallized as described previously [19]. Crystallization drops were made by mixing of 3 μl of protein solution (5–7 mg/ml) with 1 μl of precipitant solution consisting of 0.1 M Tris-HCl pH 7.5, 0.13 M calcium acetate, and 25% (w/v) PEG 4000 by sitting drop vapour diffusion method. The drops were equilibrated against a reservoir (800 μl of precipitant solution), sealed and incubated at 277 K in CombiClover plates (Emerald Biosystems, USA) for one week. The diffraction data were collected at 100 K without any additional cryoprotection at the EMBL Hamburg beamline X11 of the DORIS storage ring (DESY, Hamburg, Germany) using the MAR 555 flat panel detector at a wavelength of 0.918 Å. The data were processed with XDS [26]. Diffraction data collection and processing statistics are summarized in Table 1.

4.11. Structure determination, refinement and validation

The crystal structure of DbeA-M1 enzyme variant was solved by molecular replacement method with MOLREP program [27], using the haloalkane dehalogenase DbeA (PDB ID 4K2A; [20]) as a search template. Model refinement was carried out using REFMAC5 [27] as a part of CCP4 software package [28], alternating with cycles of manual model building using COOT [29]. Ten TLS groups suggested by TLS motion determination server [30] and several cycles of TLS (translation-libration-screw) refinement were performed [31]. The refinement statistics are shown in Table 1. The structural representations were prepared by PYMOL (Schrödinger, LLC). The structure was deposited in Protein Data Bank under PDB code 6XY9. The quality of refined structure was validated to the experimental data by MOLPROBITY server [32], validation tools implemented in COOT [29] and SFCHECK program [33].

Data accessibility

Atomic coordinates and structure factors of the DbeA-M1 enzyme variant were deposited in the Protein Data Bank under the PDB code 6XY9. Authors will release the atomic coordinates and experimental data upon article publication.

Declaration of competing interest

The authors declare no conflict of interest.

CRediT authorship contribution statement

Martin Marek: Conceptualization, Supervision, Visualization, Writing - review & editing. **Radka Chaloupkova:** Methodology, Investigation, Conceptualization. **Tatyana Prudnikova:** Methodology, Investigation. **Yukari Sato:** Methodology, Investigation. **Pavlina Rezacova:** Methodology, Investigation. **Yuji Nagata:** Methodology, Investigation. **Ivana Kuta Smatanova:** Methodology, Investigation. **Jiri Damborsky:** Conceptualization, Supervision, Writing - review & editing, Funding acquisition.

Acknowledgements

Appendix A. Supplementary data

Supplementary data to this article can be found online at https://doi.org/10.1016/j.csbj.2020.05.019.

References

[1] Newton MS, Arcus VL, Gerth ML, Patrick WM. Enzyme evolution: innovation is easy, optimization is complicated. Curr Opin Struct Biol 2018;48:110–6.

[2] Martínez Cuesta S, Rahman S, Furnham N, Thornton JM. The classification and evolution of enzyme function. Biophys J 2015;109:1082–6.

[3] Bornscheuer UT, Huisman GW, Kazlauskas RJ, Lutz S, Moore JC, Robins K. Engineering the third wave of biocatalysis. Nature 2012;485:185–93.

[4] Singh R, Kumar M, Mittal A, Mehta PK. Microbial enzymes: industrial progress in 21st century. 3 Biotech 2016;6. 174-174.

[5] Sheldon RA, Woodley JM. Role of biocatalysis in sustainable chemistry. Chem Rev 2018;118:801–38.

[6] Erb TJ, Jones PR, Bar-Even A. Synthetic metabolism: metabolic engineering meets enzyme design. Curr Opin Chem Biol 2017;37:56–62.

[7] Austin HP, Allen MD, Donohoe BS, Rorrer NA, Kearns FL, Silveira RL, et al. Characterization and engineering of a plastic-degrading aromatic polyesterase. PNAS 2018;115:E4350–7.

[8] Reetz MT. Controlling the enantioselectivity of enzymes by directed evolution: practical and theoretical ramifications. PNAS 2004;101:5716–22.

[9] Chen BS, Ribeiro de Souza FZ. Enzymatic synthesis of enantiopure alcohols: current state and perspectives. RSC Adv 2019;9:2102–15.

[10] Honig M, Sondermann P, Turner NJ, Carreira EM. Enantioselective chemo- and biocatalysis: partners in retrosynthesis. Angew Chem Int Ed 2017;56:8942–73.

[11] Damborsky J, Chaloupkova R, Pavlova M, Chovancova E, Brezovsky J. Structure-function relationships and engineering of haloalkane dehalogenases. In: Timmis KN, editor. Handbook of hydrocarbon and lipid microbiology. Berlin, Heidelberg: Springer; 2010. p. 1081–98.

[12] Marek J, Vévodová J, Smatanová Kutá I, Nagata Y, Svensson LA, Newman J, et al. Crystal structure of the haloalkane dehalogenase from *Sphingomonas paucimobilis* UT26. Biochemistry 2000;39:14082–6.

[13] Kaushik S, Marques SM, Khirsariya P, Paruch K, Libichova L, Brezovsky J, et al. Impact of the access tunnel engineering on catalysis is strictly ligand-specific. FEBS J 2018;285:1456–76.

[14] Chaloupkova R, Sykorova J, Prokop Z, Jesenska A, Monincova M, Pavlova M, et al. Modification of activity and specificity of haloalkane dehalogenase from *Sphingomonas paucimobilis* UT26 by engineering of its entrance tunnel. J Biol Chem 2003;278:52622–8.

[15] Pieters RJ, Lutje Spelberg JH, Kellogg RM, Janssen DB. The enantioselectivity of haloalkane dehalogenases. Tetrahedron Lett 2001;42:469–71.

[16] Prokop Z, Sato Y, Brezovsky J, Mozga T, Chaloupkova R, Koudelakova T, et al. Enantioselectivity of haloalkane dehalogenases and its modulation by surface loop engineering. Angew Chem Int Ed 2010;49:6111–5.

[17] Chaloupkova R, Prokop Z, Sato Y, Nagata Y, Damborsky J. Stereoselectivity and conformational stability of haloalkane dehalogenase DbjA from *Bradyrhizobium japonicum* USDA110: the effect of pH and temperature. FEBS J 2011;278:2728–38.

[18] Liskova V, Stepankova V, Bednar D, Brezovsky J, Prokop Z, Chaloupkova R, et al. Different structural origins of the enantioselectivity of haloalkane dehalogenases toward linear β-haloalkanes: open-solvated versus occluded-desolvated active sites. Angew Chem Int Ed 2017;56:4719–23.

[19] Prudnikova T, Mozga T, Rezacova P, Chaloupkova R, Sato Y, Nagata Y, et al. Crystallization and preliminary X-ray analysis of a novel haloalkane dehalogenase DbeA from *Bradyrhizobium elkani* USDA94. Acta Crystallographica Section F 2009;65:353–6.

[20] Chaloupkova R, Prudnikova T, Rezacova P, Prokop Z, Koudelakova T, Daniel L, et al. Structural and functional analysis of a novel haloalkane dehalogenase with two halide-binding sites. Acta Crystallographica Section D 2014;70:1884–97.

[21] Monincova M, Prokop Z, Vevodova J, Nagata Y, Damborsky J. Weak activity of haloalkane dehalogenase LinB with 1,2,3-trichloropropane revealed by X-ray crystallography and microcalorimetry. Appl Environ Microbiol 2007;73:2005–8.

[22] Sykora J, Brezovsky J, Koudelakova T, Lahoda M, Fortova A, Chernovets T, et al. Dynamics and hydration explain failed functional transformation in dehalogenase design. Nat Chem Biol 2014;10:428–30.

[23] Koudelakova T, Chovancova E, Brezovsky J, Monincova M, Fortova A, Jarkovsky J, et al. Substrate specificity of haloalkane dehalogenases. Biochem J 2011;435:345–54.

[24] Iwasaki I, Utsumi S, Ozawa T. New colorimetric determination of chloride using mercuric thiocyanate and ferric ion. Bull Chem Soc Jpn 1952;25:226.

[25] Chen CS, Fujimoto Y, Girdaukas G, Sih CJ. Quantitative analyses of biochemical kinetic resolutions of enantiomers. J Am Chem Soc 1982;104:7294–9.

[26] Kabsch W. XDS. Acta Crystallogr Section D 2010;66:125–32.

[27] Murshudov GN, Skubak P, Lebedev AA, Pannu NS, Steiner RA, Nicholls RA, et al. REFMAC5 for the refinement of macromolecular crystal structures. Acta Crystallogr D Biol Crystallogr 2011;67:355–67.

[28] Winn MD, Ballard CC, Cowtan KD, Dodson EJ, Emsley P, Evans PR, et al. Overview of the CCP4 suite and current developments. Acta Crystallogr D Biol Crystallogr 2011;67:235–42.

[29] Emsley P, Lohkamp B, Scott WG, Cowtan K. Features and development of Coot. Acta Crystallogr D Biol Crystallogr 2010;66:486–501.

[30] Painter J, Merritt EA. TLSMD web server for the generation of multi-group TLS models. J Appl Crystallogr 2006;39:109–11.

[31] Winn MD, Murshudov GN, Papiz MZ. Macromolecular TLS refinement in REFMAC at moderate resolutions. In: Methods in enzymology. Academic Press; 2003. p. 300–21.

[32] Williams CJ, Headd JJ, Moriarty NW, Prisant MG, Videau LL, Deis LN, et al. MolProbity: more and better reference data for improved all-atom structure validation. Protein Sci 2018;27:293–315.

[33] Vaguine AA, Richelle J, Wodak SJ. SFCHECK: a unified set of procedures for evaluating the quality of macromolecular structure-factor data and their agreement with the atomic model. Acta Crystallogr Section D 1999;55:191–205.